ISSN (Print) 1226-1750
ISSN (Online) 2233-6656
**Journal of Magnetics** 24(3), 530-542 (2019) https://doi.org/10.4283/JMAG.2019.24.3.530

# Defect Detection of Oil and Gas Pipeline using Remote Field Eddy Current Technology

**Mingjiang Shi[1]*, Lin Feng[1], Zhiqiang Huang[1], Mengfei Zhang[1], Hao Wen[1], and Qing Liu[2]**

[1]*School of Mechatronic Engineering, Southwest Petroleum University, Chengdu 610500, China*
[2]*Karamay Jianye Energy Co., Ltd., Karamay 834000, China*

(Received 18 February 2019, Received in final form 16 August 2019, Accepted 27 August 2019)

**To solve the problem of wall thickness reduction and defects of oil and gas pipeline caused by corrosion or erosion, a remote field eddy current (RFEC) testing method with coaxial double coil structure is proposed to detect corrosion residual wall thickness of oil and gas gathering pipelines. Based on electromagnetic field theories, RFEC technology is theoretically analyzed. The theoretical model of RFEC detection for coaxial double coil structure is established. The relationship between the voltage phase of detection signal and the wall thickness of pipeline is derived, and an evaluation method of the residual wall thickness of the pipeline based on the phase trough time of the RFEC detection signal is proposed. The parameters of RFEC probe are optimized by Finite Element Method, and the detection system is designed on the basis of it. The practicability and the correctness of the theoretical model of the detection system are verified by experiments. It can be used to detect the residual wall thickness of pipelines in real time under different media conditions.**

**Keywords :** pipeline, defection, remote field eddy current, optimization design

## 1. Introduction

In oil and natural gas industry, collection and transportation pipeline transports the untreated mixed substances, such as oil and natural gas produced from various scattered oil fields to oil and gas treatment stations. Therefore, the pipeline of oil and gas transport is long and the pipeline network layout is complicated. Meanwhile, the crude oil flowing through the pipeline is a complex and varied medium, which is highly corrosive. It makes the oil and gas gathering pipeline easily being corroded and damaged, forming defects and affecting the safe production of oil and gas gathering stations [1]. They are divided into the corrosion of the inner wall of the pipe and the corrosion of the outer wall of the pipe according to the position of the corroded pipe wall [2]. The outer wall of the pipe is corroded mainly because physical, chemical and electrochemical reactions occur when the outer wall of the pipe is in contact with soil, air, water and strong sunlight for a long time, which leads to defects in the corrosion of the pipe wall. Corrosion of the inner wall of the pipe is mainly due to the gas-liquid mixture containing a large amount of corrosive gas and brine, which chemically and electrochemically interact with the inner wall of the pipe to corrode the pipe wall. In order to ensure that oil and gas gathering and transportation stations can be operated safely and efficiently, it is necessary to carry out defect detection on oil and gas gathering and transportation pipelines.

To detect oil and gas gathering pipeline defects, common methods include ultrasonic method, magnetic flux leakage method and conventional eddy current (EC) method [3]. Ultrasonic testing technology uses the propagation and reflection of ultrasonic waves in the medium to be tested to detect defect information [4]. Ultrasonic testing technology has the characteristics of good directionality and strong penetrating ability. However, the detection speed of the technology is relatively slow, and a coupling agent is needed in the detection process [5]. It is difficult to quantitatively obtain the type and size of the defect, and the detection accuracy of the small crack is not high. The magnetic flux leakage detection technology uses an external magnetic field (MF) to magnetize the ferromagnetic material, and the magnetic lines of force pass through the inside of the material. If the interior of the material is intact, the distribution of the magnetic lines of the force


*Corresponding author: Tel: +86-28-8303-7203
Fax: +86-28-8303-7203, e-mail: swpushi@126.com

within the material will be relatively uniform, and the detecting sensor does not receive the leakage MF signal. If there are defects such as corrosion or crack inside the material, the magnetic lines of the force passing through the defect area will be distorted due to the change of the magnetic resistance of the material, and some of them will pass through the surface of the material, so that the formation near the outer surface of the defect can be detected by the detecting sensor [6]. Magnetic flux leakage detection is relatively efficient because it requires low surface cleaning of the detector. However, there are many disturbances in the detection process, leading to uncertainty in its inversion, that is, there is no unique solution. The EC detection technology adopts the principle of electromagnetic detection. When an alternating current signal is applied to exciting coil, a varying excitation MF is generated in the vicinity of the coil. Then the ferromagnetic detected test piece is brought close to, and an induced current is generated in the test piece. The MF generated by the EC is opposite to the excitation MF, and the frequency is the same. It is called the reflected MF. The reflected MF acts on the detecting coil, which changes the impedance of the detecting coil. The metal defect related information can be determined by measuring the impedance change of the detecting coil. This is the most common EC testing method. Due to the skin effect, the conventional EC can only detect pipe surface and near surface defects.

The RFEC technique uses a low-frequency excitation signal [7]. Under low-frequency excitation conditions, a RFEC phenomenon occurs in a certain distance from the exciting coil. This EC phenomenon is different from the conventional EC phenomenon [8]. Part of the MF energy generated by the exciting coil passes through the tube wall twice and carries the inner and outer tube wall information to the receiving coil [9]. Therefore, RFEC technology has the following advantages in the detection of pipe wall defects: it is not affected by the non-metallic coating on the weld surface. The detection sensitivity of corrosion defects on inner and outer tube walls is consistent. The thickness of tube wall is approximately proportional to the phase of detection signal, so it is easy to distinguish defects. It inherits the advantages of non-contact, high sensitivity and fast detection speed of traditional EC method. Compared with conventional eddy current inspection, RFEC method not only has the potential to overcome the lift-off effects, but also has the ability to detect the inner defect for thick ferromagnetic pipes [10].

This paper aims at the actual problem that oil and gas gathering and transportation pipelines are prone to corrosion and defects. Based on the flaw detection mechanism of RFEC pipeline, a simulation model of flaw detection is established and a simulation experiment is conducted [11]. According to the distribution of MF in the pipeline, the exciting coil and detecting coil are designed, and the probe length is optimized. For the different defects of pipe, the internal relation between defect depth and detecting signal phase is analyzed, and the defect depth is quantitatively identified. On the basis of the simulation, the detection system was built and the pipeline defect detection experiment was carried out to verify the relationship between defect depth and signal phase in the theoretical model and the simulation model.

## 2. Detection Principle

### 2.1. Principle of RFEC testing technology

RFEC is a low-frequency EC detection technology that can penetrate the metal pipe wall twice [12]. Its detection principle is shown in Fig. 1. The main structure of the RFEC probe includes the exciting coil coaxially placed with the pipeline and the detection coil coaxially placed in the remote field region (RFR), as well as some parts for improving the detection performance of the probe, such as shielding device, magnetic conductive device, magnetic saturation device, etc. [13].

After the low-frequency sinusoidal alternating current is applied into the exciting coil [14], three typical RFEC in the near field region (NFR), the transition region (TR) and the RFR are formed in the pipeline. Meanwhile, energy direct flow paths will occur in the pipeline, and energy indirect flow paths will occur near the wall. In the NFR, the alternating MF generated by the exciting coil is relatively strong. However, with the increase of axial distance from the exciting coil, the magnetic field intensity (MFI) decreases sharply due to the shielding effect of the induced EC in the pipe wall near the exciting coil, and the MF distribution in this region cannot contribute to the defect detection signal. The exciting coil and its adjacent

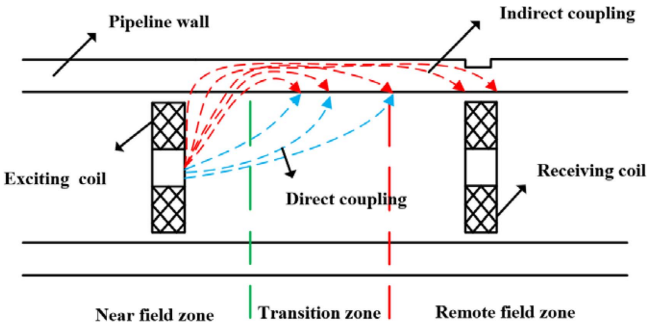


**Fig. 1.** (Color online) Schematic diagram of RFEC defect detection principle.

pipe wall form a transformer structure, and a circumferential EC is generated in the pipe wall. Some of the EC rapidly diffuses to the outer surface of the pipe, and these circumferential EC further produce the alternating MF which diffuses into the air near the wall of the tube and conducts along the tube to the remote field [15]. The indirect energy in the remote field is much greater than the direct energy. Therefore, the MF outside the pipe passes through the pipe wall again and enters the RFR. The MF in the RFR that passes through the pipe wall twice contains the defect information of the pipe wall, which can be identified and found by the detection coil.

Compared with the excitation signal, the detection signal in the RFR has a phase lag, which can be obtained from the one-dimensional skin effect [16]:

$$\theta = 2h\sqrt{\pi h\mu\sigma} \tag{1}$$

In the above formula, $\theta$ is the phase lag of the induced potential, $h$ is the measured wall thickness, $f$ is the detecting the excitation frequency, $\mu$ is the magnetic permeability of the material of the pipe wall, and $\sigma$ is the electrical conductivity of the material of the pipe wall. As can be seen from equation (1), when using RFEC to detect pipe defects, as long as the phase information of detection signal is obtained, the thickness information of pipe wall can be calculated. Then compared with the normal wall thickness, the measured pipe wall has defects can be known.

### 2.2. Mathematical model of RFEC pipeline defect detection

RFEC is a low-frequency electromagnetic field detection technology, and the low-frequency can be seen as the superposition of multiple steady-state [17]. According to the steady-state Maxwell equations, it can be obtained that [18]:

$$\begin{cases} \nabla \times \boldsymbol{H} = \boldsymbol{J}_c + \boldsymbol{J}_e \\ \nabla \times \boldsymbol{E} = -j\omega\boldsymbol{B} \\ \nabla \cdot \boldsymbol{B} = 0 \\ \nabla \cdot \boldsymbol{D} = \rho \end{cases} \tag{2}$$

Where $\boldsymbol{H}$ is the MFI, $\boldsymbol{B}$ is the magnetic induction intensity (MII), $\boldsymbol{D}$ is the electric displacement vector, $\boldsymbol{E}$ is the electric field intensity, $\rho$ is the electric current density, $\boldsymbol{J}_c$ is the applied exciting current density, and $\boldsymbol{J}_e$ is the EC density [19].

According to the MF theory:

$$\boldsymbol{D} = \varepsilon\boldsymbol{E},\ B = \mu\boldsymbol{H},\ \boldsymbol{J}_e = \sigma\boldsymbol{E} \tag{3}$$

The vector magnetic potential is defined as $A$, and the coulomb standard shows that:

$$\nabla \times \boldsymbol{A} = \boldsymbol{B} \tag{4}$$

$$\nabla \cdot \boldsymbol{A} = 0 \tag{5}$$

Substitute equation (4) into equation (2) to obtain:

$$\nabla \times (\boldsymbol{E} + j\omega\boldsymbol{A}) = 0 \tag{6}$$

Based on irrotationality, electric scalar potential function $\varphi$ is defined:

$$\boldsymbol{E} + j\omega\boldsymbol{A} = -\nabla\varphi \tag{7}$$

Hence,

$$E = -(\nabla\varphi + j\omega\boldsymbol{A}) \tag{8}$$

Substituting equations (3), (4), and (8) into Maxwell equations (2):

$$\left[\nabla \times \frac{1}{\mu}(\nabla \times \boldsymbol{A})\right] = \boldsymbol{J}_c - \sigma(\nabla\varphi + j\omega\boldsymbol{A}) \tag{9}$$

From the isotropy of the material, and according to the coulomb standard and vector equation, it can be gained [20]:

$$\nabla^2\boldsymbol{A} = -\mu\boldsymbol{J}_c + \mu\sigma(\nabla\varphi + j\omega\boldsymbol{A}) \tag{10}$$

According to Maxwell equations:

$$\nabla \times \boldsymbol{J} = -\frac{\partial\rho}{\partial t} \tag{11}$$

Substitute equation (8) into equation (11) to obtain:

$$-\nabla \cdot \sigma(\nabla\varphi + j\omega\boldsymbol{A}) = -\frac{\partial\rho}{\partial t} \tag{12}$$

If displacement current is ignored, then $\frac{\partial\rho}{\partial t} = 0$, and $\sigma$ is isotropic and constant, then:

$$\nabla \cdot (\nabla\varphi + j\omega\boldsymbol{A}) = 0 \tag{13}$$

Given boundary conditions, $A$ and $\varphi$ can be obtained by computing equations (10) and (13). Furthermore, it can be gained [21]:

$$\boldsymbol{B} = \nabla \times A \tag{14}$$

$$\boldsymbol{J}_e = -\sigma(\nabla\varphi + j\omega\boldsymbol{A}) \tag{15}$$

In the case of no defects, the RFEC model of ferromagnetic pipeline presents axial symmetry [22], and the vector magnetic potential $A$ only has circumferential component $\boldsymbol{A}_\theta$, and $\frac{\partial\boldsymbol{A}_\theta}{\partial\theta} = 0$. In the RFEC, only the current source $\boldsymbol{J}_{c\theta}$ exists in the exciting coil, then $\frac{\partial\varphi}{\partial\theta} = 0$. The mathematical model of the RFEC is [23]:

$$\frac{\partial^2\boldsymbol{A}_\theta}{\partial r^2} + \frac{1}{r}\frac{\partial\boldsymbol{A}_\theta}{\partial r} + \frac{\partial^2\boldsymbol{A}_\theta}{\partial z^2} - \frac{\boldsymbol{A}_\theta}{r^2} = -\mu\boldsymbol{J}_{c\theta} + j\omega\mu\sigma\boldsymbol{A}_\theta \tag{16}$$

From equation (16), $\boldsymbol{A}_\theta$ can be solved, and the axial component of MII $B_r$ can be further obtained:

$$\boldsymbol{B}_r = -\frac{\partial \boldsymbol{A}_\theta}{\partial z} \tag{17}$$

The axial component of MII $B_z$:

$$\boldsymbol{B}_z = \frac{\boldsymbol{A}_\theta}{r} + \frac{\partial \boldsymbol{A}_\theta}{\partial r} \tag{18}$$

In the cylindrical coordinate system, through the derivation of the above formula and the definition and calculation of each parameter, we can master the relationship between a large number of parameters. Where $r$ is the radial direction of the pipeline, $z$ is the axial direction of the pipeline, and $A_\theta$ is the circumferential component of the vector magnetic potential on the coil wire. Both axial component $Bz$ and radial component $Br$ of magnetic field in the pipeline are closely related to $A_\theta$. The theoretical basis of RFEC can be clearly understood from the formula, which lays a firm foundation for subsequent research.

### 2.3. Comparison of axial and radial components of MF in tube

The amplitude and phase of the axial component $\boldsymbol{B}_z$ of the MII in the pipeline and the component $\boldsymbol{B}_r$ of the MII in the pipeline diameter are simulated and analyzed when the detection point gradually moves away from the exciting coil, as shown in Fig. 2.

It can be seen from Fig. 2 that the amplitude and phase of $\boldsymbol{B}_z$ and $B_r$ are consistent with the trend of the detection point gradually moving away from the exciting coil, and the difference between the amplitude and phase curves of the two MF components is also obvious. In Fig. 2(a), the amplitude of $\boldsymbol{B}_z$ on the axis of the pipe is 8 orders of magnitude larger than the amplitude of $\boldsymbol{B}_r$. In Fig. 2(c), the amplitude of $\boldsymbol{B}_z$ near the inner wall of the pipe is 2 orders of magnitude larger than that of $\boldsymbol{B}_r$. In the detection of EC defects, it is easier to detect the radial component $\boldsymbol{B}_z$ than the $\boldsymbol{B}_r$ detection. Meanwhile, it can be seen in Fig. 2(a) and Fig. 2(c) that if the axial component $\boldsymbol{B}_z$ of the MFI induced by the detection coil is compared with the radial component $\boldsymbol{B}_r$, the RFR will be about 0.5 times the inner diameter of the pipe in advance, which is beneficial for reducing the length of the RFEC detection probe. In

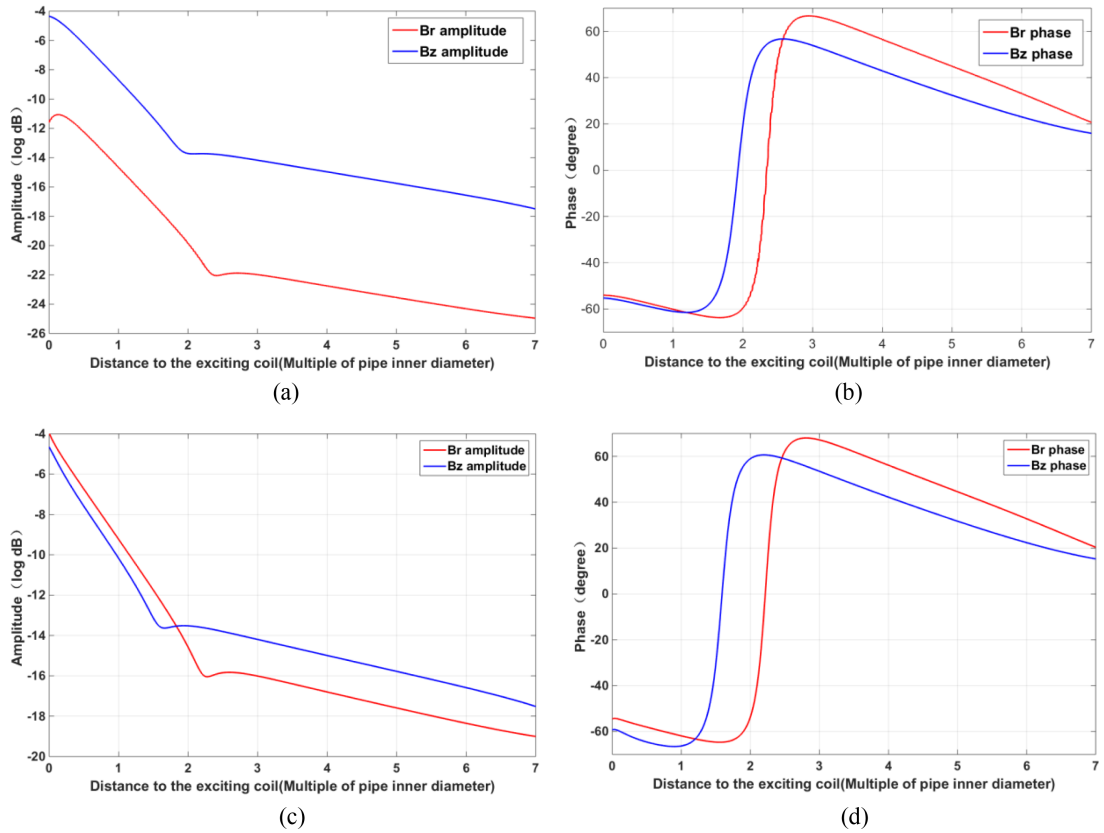


**Fig. 2.** (Color online) Amplitude and Phase Change Curves of Magnetic Induction Intensity Components: (a) Amplitude change on the axis of the pipe; (b) Phase change on the axis of the pipe; (c) Amplitude change near the inner wall of the pipe; (d) Phase change near the inner wall of the pipe

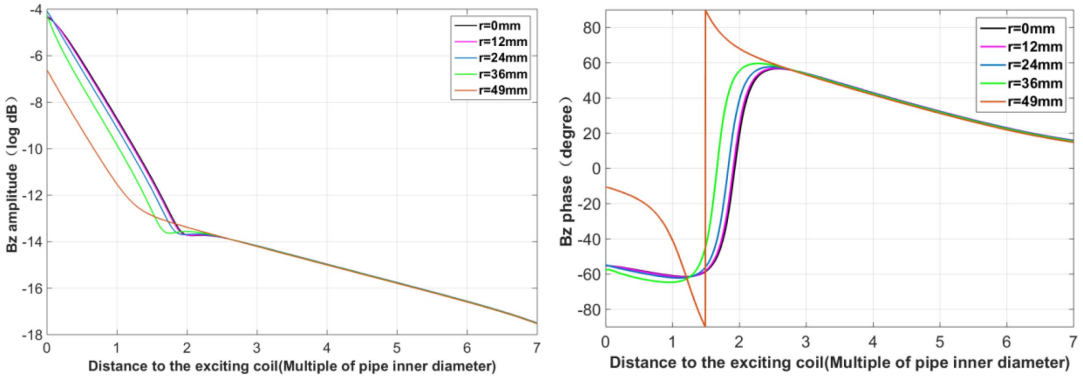


(a) (b)

**Fig. 3.** (Color online) $\boldsymbol{B}_z$ amplitude and phase change curves when detection points are located in different radial positions: (a) $\boldsymbol{B}_z$ amplitude change curve when detection point is at different radial positions; (b) $\boldsymbol{B}_z$ phase change curve when the detection point is at different radial positions

Fig. 2(b) and Fig. 2(d), the phase and amplitude changes of the two MII components are close to each other. Compared with the $\boldsymbol{B}_r$ phase change curve, the $\boldsymbol{B}_z$ phase change curve also appears in the RFR about 0.5 times earlier than the pipe inner diameter. Therefore, the MII axial component $\boldsymbol{B}_z$ was selected by the detection system for research.

It can be seen from Fig. 2 that the RFR is also advanced when the RFEC detection point is located near the inner wall of the tube, compared with the detection point on the axis of the tube. In order to analyze this phenomenon deeper, the detection points are obtained using simulation between the axis of the pipe (y = 0 mm), the axis of the pipe and the inner wall of the pipe (y = 12 mm, y = 24 mm and y = 36 mm) and the inner wall of the pipe (y = 49 mm). The axial component of the MF strength $\boldsymbol{B}_z$ gradually drifts away from the amplitude and phase change curve of the exciting coil as the detection point, as shown in Fig. 3.

It can be seen from Fig. 3 that the closer the position of the detection point is to the inner wall of the pipe, the earlier the amplitude and phase change curves enter the RFR. Meanwhile, it can be found that when the detection point moves from the axis of the pipe to the inner wall of the pipe, the speed of the forward remote field portion of each curve is different. When the detection point moves in an equidistant radial direction near the axis of the pipeline, the remote field advance speed is slower on the amplitude and phase change curve, while the remote field advance speed is faster on the amplitude and phase change curve when the detection point moves in an equidistant radial direction near the inner wall of the pipeline.

### 2.4. Influence of medium in tube on MF

The medium of oil and gas collection and transportation pipeline is mainly a mixture of oil, water and natural gas. The influence of the presence of these media on the MF distribution is analyzed here. The conductivity of oil is

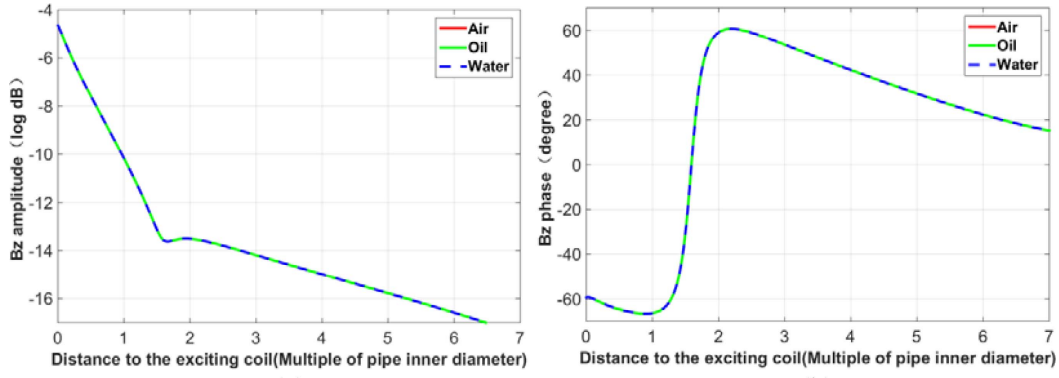


(a) (b)

**Fig. 4.** (Color online) Comparison of $\boldsymbol{B}_z$ amplitude and phase under different media in the pipe: (a) $\boldsymbol{B}_z$ amplitude contrast curves in different media; (b) $\boldsymbol{B}_z$ phase contrast curves in different media

about 100 to 200 microns; the conductivity of common water is about 600 microns; the conductivity of natural gas is almost 0 microns. The comparison curve of the axial component ***B***z amplitude and phase of the MII in the pipe in air, oil and water is obtained through simulation, as shown in Fig. 4.

As can be seen from Fig. 4, when there are three different media, water, oil and air, respectively, in the pipe, the amplitude and phase curves of the axial component ***B***z of the MII completely coincide. Therefore, the presence of oil, water, natural gas and other media in the pipeline will not have an impact on the detection results.

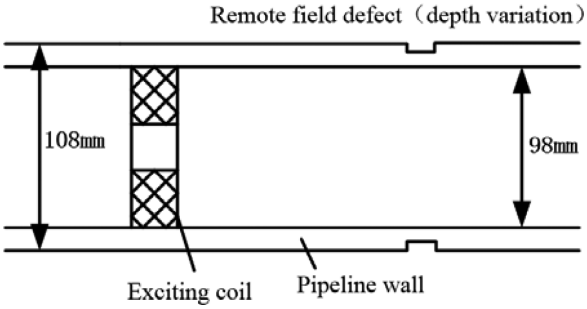


**Fig. 5.** (Color online) Schematic diagram of defect establishment in the remote field.

### 2.5. Simulation of full-circumference axial symmetry defect detection

#### 2.5.1. Model establishment and analysis of simulation results

In this paper, the finite element simulation software is used to carry out simulation experimental research on the magnetic field distribution of RFEC in the pipe, the axial and radial components of magnetic field in the pipe, the magnetic field distribution under the full circumferential axisymmetric groove defect, the relationship between defect depth and magnetic field signal, and the relationship between internal and external wall defect signal. Finite element analysis is carried out in the following steps: (1) Element subdivision: the object to be solved is divided into finite geometric elements, and the adjacent elements are connected by multiple nodes. (2) Element analysis: piecewise interpolation. The unknown function of any point in the corresponding partitioning unit is expanded by the shape function in the partitioning unit and the function value at the discrete mesh point, and the linear interpolation function is established. (3) Establishing and solving the approximate variational equation: According to the energy equation or the weighted residuals equation, a finite set of algebraic equations with undetermined parameters can be established, and the numerical solution of the differential equation can be obtained by solving the discrete equations. (4) Post-processing: Calculate the derived results according to the specific problems we need to study.

Using the RFEC detection principle, a finite element model of the pipeline defect as shown in Fig. 5 is established. The pipe has an outer diameter of 108mm, an inner diameter of 98 mm, a defect width of 5mm, and a depth of 1 mm, 2 mm, 3 mm, and 4 mm. The simulation results show that the amplitude and phase of $\boldsymbol{B}_z$ gradually move away from the exciting coil with the detection point as shown in Fig. 6.

It can be seen from Fig. 6 that when the depth of the defect is different, the amplitude and phase curve of $\boldsymbol{B}_z$ change differently. The deeper the defect is, the more obvious the curve changes. At the 3 times pipe diameter, the variation is the largest. In Fig. 6(a), the change in $\boldsymbol{B}_z$ amplitude is around $10^{-14}$, and it is difficult to accurately measure the signal, which is likely to cause large errors. In Fig. 6(b), the variation of the $\boldsymbol{B}_z$ phase curve is

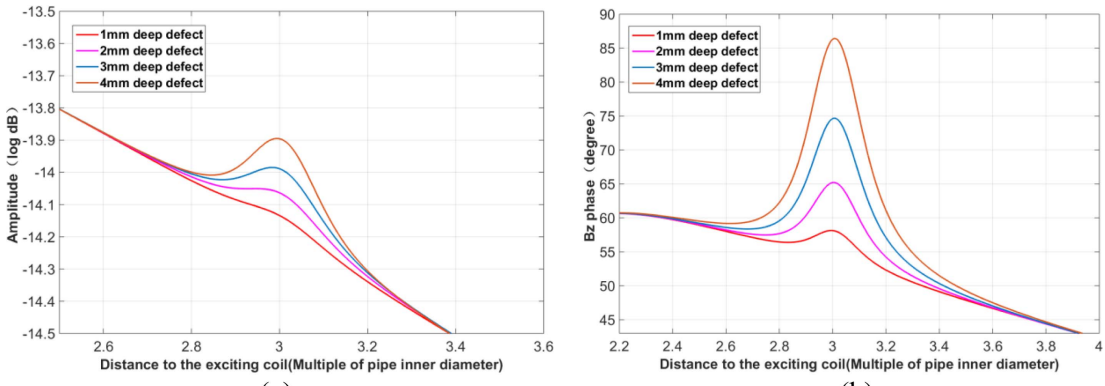


(a) (b)

**Fig. 6.** (Color online) Comparison of $\boldsymbol{B}_z$ amplitude and phase curves under different depth defects: (a) $\boldsymbol{B}_z$ amplitude contrast curve under different depth defects; (b) $\boldsymbol{B}_z$ phase contrast curve under different depth defects

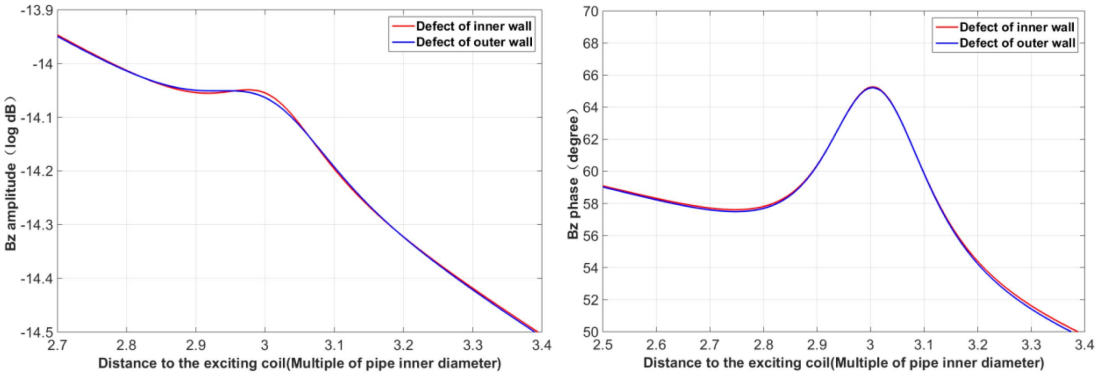


(a) (b)

**Fig. 7.** (Color online) Comparison of $\boldsymbol{B}_z$ amplitude and phase under inner and outer wall defects: (a) Amplitude contrast of $\boldsymbol{B}_z$ under inner and outer wall defects; (b) Phase contrast of $\boldsymbol{B}_z$ under inner and outer wall defects

between several degrees and several tens of degrees, and the variation range is large, so that it is possible to distinguish whether there is a defect. Therefore, in the RFEC testing of pipeline defects, the change of the phase of the detection signal is more reliable as the main defect analysis signal, and the signal amplitude change can be used as the auxiliary analysis signal.

2.5.2. Comparative analysis of internal and external wall defects simulation

Because of the actual working condition, the defects of the oil and gas gathering and transportation pipeline may appear on the inner and outer walls of the pipeline. For the same parameter defect, the center of the defect is still 3 times the inner diameter of the tube from the exciting coil, and the depth and width of the defect are 2mm and 5mm respectively. The simulation is carried out for the defect in the outer wall of the pipe and the inner wall of the pipe, and a comparison chart of the amplitude and phase change curve of $\boldsymbol{B}_z$ is obtained, as shown in Fig. 7.

It can be seen from Fig. 7 that when the same defect exists in both the outer wall of the pipe and the inner wall of the pipe, the amplitude and phase curves of the axial component $\boldsymbol{B}_z$ of the MII at the defect are substantially coincident, and the amount of protrusion change is also the same. It can be seen that when the RFEC technology is used to detect the defect of the pipe wall, the sensitivity of detecting the defects of the outer wall and the inner wall of the pipe is consistent.

### 2.6. Simulation with shielded disk

The length of the detection system is required to be short, because of the large number of bend sections and small radius of curvature of oil and gas pipelines. However, the length of the RFEC detection probe is long, and it is difficult for the probe to pass through the pipeline in the process of defect detection. Therefore, magnetic shielding disk is added between the detection coil and the exciting coil to reduce the length of the detection system. In the phenomenon of RFEC, there are two energy flow

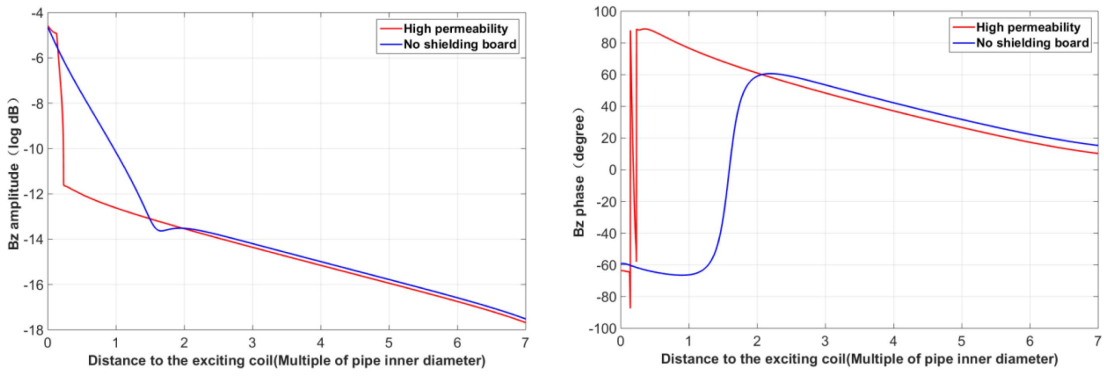


(a) (b)

**Fig. 8.** (Color online) Comparison of $\boldsymbol{B}_z$ amplitude and phase curves under the high permeability shielding plate; (a) Comparison of $\boldsymbol{B}_z$ amplitude curves with or without shielding plates; (b) Comparison of $\boldsymbol{B}_z$ phase curves with or without shielding plates

paths from the exciting coil to the detection coil, one is the direct energy coupling path in the pipe, and the other is the indirect coupling path from the exciting coil to the outside of the pipe and then from the outside to the RFR in the pipe. Shield plate is added near the exciting coil in the pipe to accelerate the attenuation of MF energy on the direct coupling path, so that the energy of the indirect coupling path is faster and stronger than that of the direct coupling path. In this way, the RFR is advanced, and the NFR and TR are shortened. The shielding plate is mainly composed of copper plate, aluminum plate and other high conductivity materials and silicon steel plate and other high permeability materials. The amplitude and phase change curves of $\boldsymbol{B}_z$ after adding the shielding plate are shown in Fig. 8(a), (b)

As can be seen from Fig. 8, the amplitude and phase curves of $\boldsymbol{B}_z$ begin to enter the RFR at about 0.5 times the inner diameter of the tube. Meanwhile, in the newly formed NFR and TR, the amplitude attenuation is faster and the phase change is more drastic. Compared with the amplitude and phase curves of $\boldsymbol{B}_z$, when there was no shielding disk, the RFR was approximately 1.5 times the inner diameter of the pipe after adding a shielding disk with high permeability near the exciting coil.

## 3. The Experiment

The block diagram of the pipeline defect detection system based on remote field EC technology is shown in Fig. 9. The detection system is mainly composed of the incentive source of low-frequency sine signal, incentive signal power amplification, RFEC detection probe, pipe to be tested, defect signal conditioning and acquisition module, phase sensitive detection module for processing signal amplitude and phase, and man-machine interaction module for detection signal display.

The two most critical parts of the RFEC testing probe

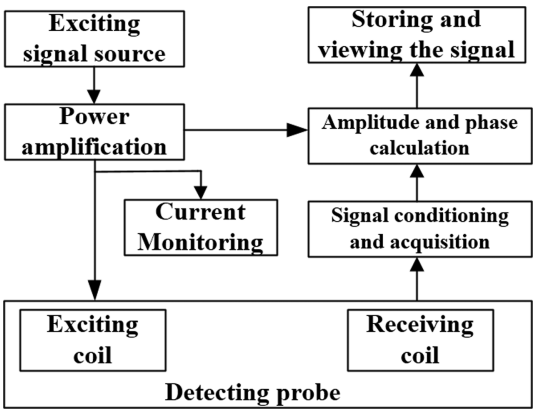


**Fig. 9.** Structure block diagram of the RFEC detection system.

are the exciting coil and the receiving coil. The exciting coil is placed in coaxial with the pipe, and the receiving coil is placed in the remote field with a certain distance from the exciting coil. The receiving coil can be in a form similar in size to the exciting coil and coaxial with the pipe, or in a form of small coils arranged circumferentially around the inner wall of the pipe. In this paper, two types of receiver coils are compared and analyzed.

## 4. Design of Exciting Coil Parameters

Due to the large diameter and thick wall of the oil and gas gathering and transportation pipeline, the electromagnetic field generated by the exciting coil is weak after it passes through the pipe wall twice to the remote field. Therefore, the exciting coil needs to be optimally designed to generate a large excitation MF in a limited design space. Parameters of the exciting coil are set as follows: outer diameter of the coil D1 = 86 mm, inner diameter of the coil d1 = 50 mm, coil thickness h1 = 15 mm, number of turns of the coil N1 = 350, DC resistance R1 = 6.2Ω, outer diameter of the skeleton D2 = 90 mm, and inner diameter of the skeleton d2 = 20 mm.

### 4.1. Design of receiving coil parameters

When the detection probe passes through a defect, the receiving coil senses a MF that changes near the defect to enable the defect detection. The receiving coil is placed in a RFR at a distance from the exciting coil for sensing the MF signal of the tube wall information in the RFR. The receiving coil has a form similar to the exciting coil and placed coaxially with the pipe to be tested, and also has an array of small coils arranged circumferentially around the inner wall of the tube. The large receiving coil, which is similar in size to the exciting coil and coaxially placed, has a large volume, a large number of turns and a large MF range to be sensed. A small receiving coil arranged circumferentially around the wall of the tube is relatively small in volume, and the MF range that can be felt is mainly the small MF at the position of the coil.

When the circumferential defects (especially the circumferential defects) are detected, the output signal amplitude of the large receiving coil is relatively large. When detecting the small area defect on the pipe wall, the small receiving coil has higher sensitivity. Since the large receiving coil recognizes the average situation in which the defect occupies the entire circumference of the pipe wall, when the defect is small, the output defect signal of the large receiving coil will be small.

In this experimental design, the receiving coil was designed in three different forms. The first type is a form

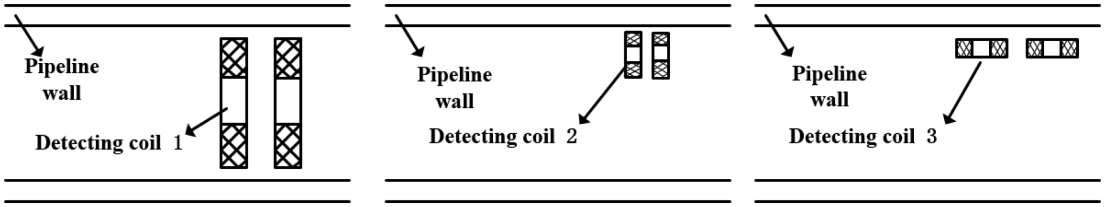


**Fig. 10.** The form and placement of the detection coil.

**Table 1.** Three types of coil parameters table.

| | Outer diameter (mm) | Inner diameter (mm) | Thickness (mm) | Number of turns | Resistance (Ω) | Placement method |
|---|---|---|---|---|---|---|
| Coil No.1 | 86 | 70 | 10 | 1700 | 465 | The central axis of the coil is coaxial with the central axis of the pipe |
| Coil No.2 | 20 | 12 | 3.5 | 1200 | 125 | The central axis of the coil is parallel to the central axis of the pipe |
| Coil No.3 | 20 | 12 | 3.5 | 1200 | 125 | The center axis of the coil is perpendicular to the center axis of the pipe |

similar to the size of the exciting coil and placed coaxially with the pipe; the second type is placed in the form of a small receiving coil near the inner wall of the pipe, the central axis of the coil is parallel to the axis of the pipe. Like the first kind of coil, we can feel the change of the axial component $\boldsymbol{B}_z$ of the MII in the remote field. Compared with the second type, the third class has the same coil parameters, but is placed in a form perpendicular to the central axis of the coil and the axis of the pipe. The plane of the coil is parallel to the cut surface of the pipe wall, and we can feel the change of the radial component $\boldsymbol{B}_r$ of the MII in the RFR.

### 4.2. Comparison of detection capability of three types of probes

Two kinds of different groove defects were set to carry out a comparative experiment on the detection ability of different forms of receiving coils. One is a full-circumference axial symmetric defect, the flaw parameter is 5 mm in axial width and 3 mm in radial depth. One is the locally oriented groove defect, whose parameters are axial width 5 mm, circumferential length 20 mm and radial depth 3 mm, as shown in Fig. 11.

Three types of different forms of detection probes were used to detect the two kinds of defects, and the detection signals were obtained as shown in Fig. 12, and the amplitude and phase information of these defect signals were summarized in Table 2.

It can be seen that different forms of receiving coils have different detection capabilities for the same defect. No matter which type of receiving coil is used to detect the two defects shown in Fig. 12, the ability to detect the circumferential defects is better than that of the circumferential local defects. In addition, when the defect depth is consistent, the phase of the detection signal is basically the same, which indicates that there is a certain relation-

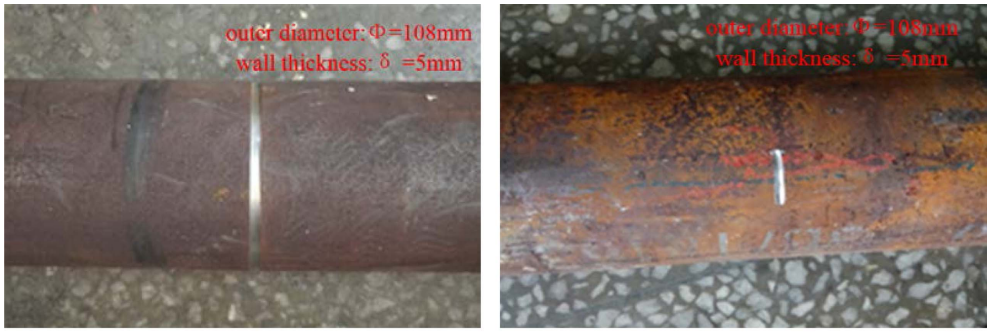


(a) (b)

**Fig. 11.** (Color online) Defective pipeline: (a) Steel tube with full-circumference axial symmetry defect; (b) Steel tube with local groove defect groove.

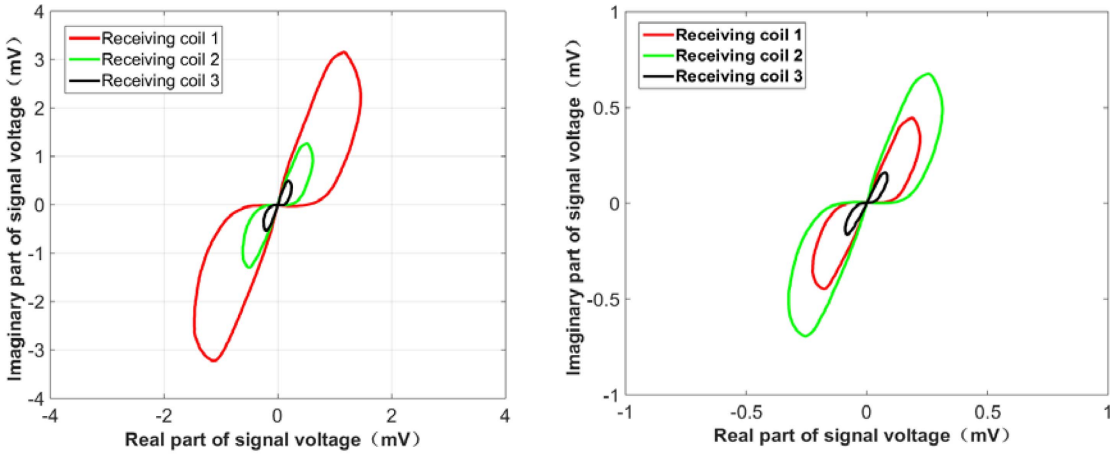


**Fig. 12.** (Color online) Contrast diagram of two defect detection signals: (a) Comparison of the detection of the full-circumference defect signal by different coils; (b) Comparison of the detection of the local circumferential defect signal by different coils

**Table 2.** Amplitude and phase values of defect detection of receiving coils in different forms.

| | Full-circumferential axisymmetric groove defect | | Circumferential local groove defect | |
|---|---|---|---|---|
| | Amplitude (mV) | Phase (degree) | Amplitude (mV) | Phase (degree) |
| the 1st type of receiving coil | 6.72 | 73.82 | 0.90 | 74.33 |
| the 2nd type of receiving coil | 2.11 | 75.15 | 1.36 | 74.24 |
| the 3rd type of receiving coil | 0.78 | 74.91 | 0.33 | 73.53 |

ship between the defect depth and the signal phase.

It can be seen from Fig. 12 and Table 2 that the first type of receiving coil is the most sensitive to the full-circumference defect, and the second type of receiving coil is the most sensitive to the circumferential local defect of the tube wall, because the first type of receiving coil recognizes the average condition of the circumferential wall where the defect occupies the whole. The second type of receiving coil recognizes the fact that the defect occupies a small portion of the arc wall. Therefore it is easier to identify a small defect signal using a small coil, and the sensitivity and resolution of the circumferential defect are higher. In the case of the above two defects, the defect detection ability of the third type receiving coil are inferior to the first type and the second type of receiving coils. This is because the MF in the remote field is dominated by the axial direction of the pipeline, and the disturbance caused by the defect to the MF is most drastic in the axial MF. After comparison, the RFEC probe made of the second type of receiving coil was used in the subsequent experiments.

### 4.3. Comparison of different types of defect detection capabilities

In the actual working condition, there are basically no full-circumferential defects in the defects, and defects are generally found in the pipeline. In the laboratory test of pipeline defects, the experimental analysis is carried out by using groove defects extending in the circumferential direction, groove defects extending in the direction of the

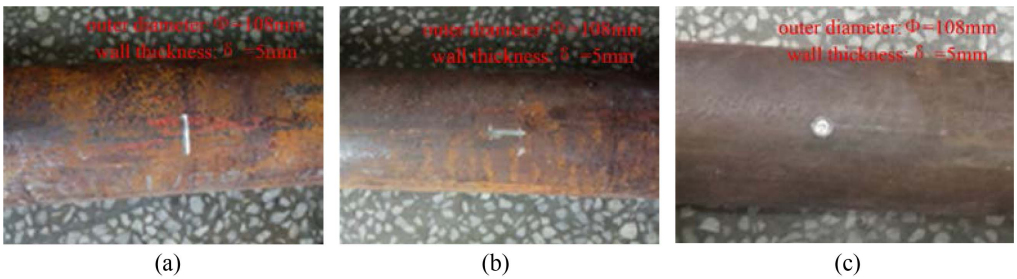


**Fig. 13.** (Color online) Three typical types of pipeline defects: (a) Circumferential groove; (b) Axial groove; (c) radial circular hole

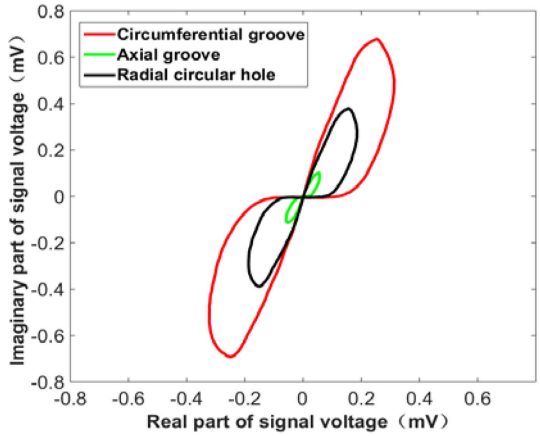


**Fig. 14.** (Color online) Comparison of different types of defect detection signals.

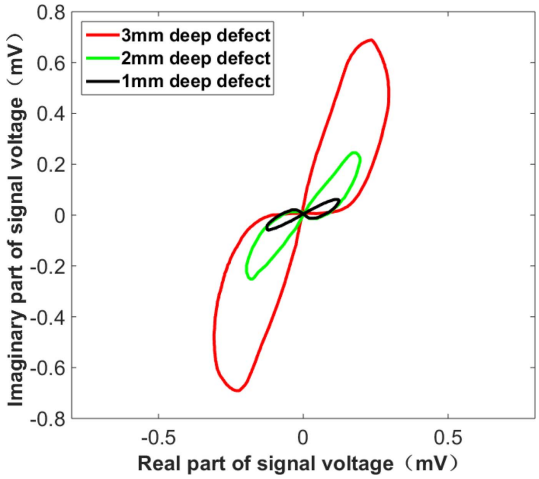


**Fig. 15.** (Color online) Contrast chart of CG defect detection signals in different depths.

**Table 3.** Amplitude and Phase of Defect Detection Signals with Different Shapes.

| | Amplitude (mV) | Phase (degree) |
|---|---|---|
| CG | 1.36 | 74.24 |
| AG | 0.25 | 73.93 |
| RCH | 0.81 | 72.71 |

central axis of the pipe, and radial circular hole. The characteristics of the three types of defects can represent large partial defects. The pictures of the above three types of defects processed is shown in Fig. 13.

The defect processing parameters are as follows:

Circumferential groove (CG): axial length 5 mm, circumferential width 20 mm, radial depth 3 mm, defect volume 300 $mm^3$.

Axial groove (AG): axial length 20 mm, circumferential width 5 mm, radial depth 3 mm, defect volume 300 $mm^3$.

Radial circular hole (RCH): diameter 11 mm, radial depth 3mm, defect volume 285 $mm^3$.

The detection coil output voltage signal is shown in Fig. 14, and the input voltage amplitude and phase are shown in Table 3.

It can be seen from Fig. 14 and Table 3 that the CG defect signal voltage amplitude is the largest, the RCH signal is the second, and the AG is the smallest. It is indicated that in the RFEC detection, the axially extended defects are the least likely to be detected, and the circumferentially extended defects are easier to detect.

### 4.4. Signal analysis of defect detection at different depths

4.4.1. Signal Analysis of CG Depth Change

In the defect detection, defect depth is a crucial information, which directly determines the remaining life of the inspected section. For the CG defect shown in Fig. 13(a), three different depths of 3 mm, 2 mm and 1 mm along the pipeline diameter direction are machined, and the other parameters of the defect remain unchanged. The CG with three different depths are detected and the detection signals are shown in Fig. 15.

As can be seen from Fig. 15, as the radial depth of the defect becomes smaller, the detection coil output signal gradually becomes smaller, and the signal as a whole is deflected. This shows that when the depth of the defect changes, the amplitude and phase of the corresponding detection signal change. In order to explain the relationship between the depth of the defect and the amplitude and phase of the detected signal, the amplitude and phase of the defect signal in Fig. 13(a) are counted in Table 4.

It can be seen from Table 4 that as the depth of the defect increases, the amplitude of the detection signal voltage increases, and the phase of the signal voltage becomes larger. The depth of the CG defect is proportional to the phase of the detection signal voltage, and the amplitude of the detection signal has an approximate exponential relationship with the depth of the defect. The deeper the defect, the larger the amplitude of the signal increases.

**Table 4.** The amplitude and phase of CG at different depths.

| | Amplitude (mV) | Phase (degree) |
|---|---|---|
| 3 mm deep CG | 1.36 | 74.24 |
| 2 mm deep CG | 0.58 | 52.11 |
| 1 mm deep CG | 0.27 | 27.67 |

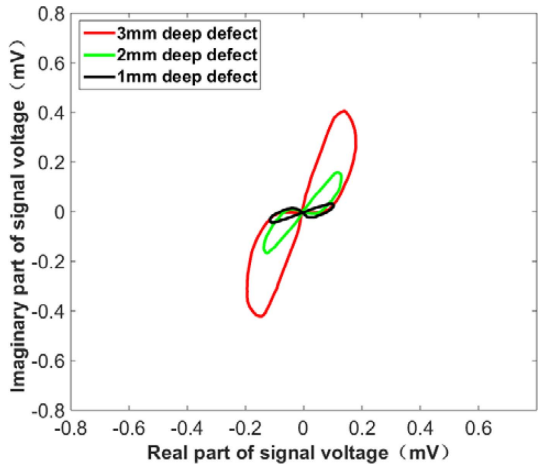


**Fig. 16.** (Color online) Contrast chart of RCH detection signals with different depths.

**Table 5.** Amplitude and phase of RCH detection signals with different depths.

| | Amplitude (mV) | Phase (degree) |
|---|---|---|
| 3 mm deep RCH | 0.81 | 72.71 |
| 2 mm deep RCH | 0.37 | 48.83 |
| 1 mm deep RCH | 0.15 | 23.55 |

4.4.2. Signal analysis of depth variation of RCH

For the RCH shown in Fig. 13(c), three different depths of 3 mm, 2 mm and 1mm are machined with the other parameters unchanged. The flaw detection signals of three circular holes with different depths are shown in Fig. 16 and Table 5.

As can be seen from Table 5, with the increase of the defect depth of the circular hole, the corresponding detection signal voltage amplitude increases, and the signal voltage phase also gradually increases. Moreover, the defect depth of the radial circular hole has an approximate exponential relationship with the voltage amplitude of the detection signal and an approximate proportional relationship with the phase of the detection signal, which is similar to the characteristics of the CG defect detection signal.

## 5. Conclusion

In this paper, the RFEC technology is used to analyze the defect detection of oil and gas gathering pipelines. The principle and mathematical theory of pipeline defect detection using RFEC technology are analyzed. The mathematical model of RFEC in pipeline is established, and the relationship between the output signal voltage of the detection coil and the MF signal is derived. The proportional relationship between the depth of the full circumferential axisymmetric groove defect and the phase change of the MF signal is simulated. In addition, the influence of the defects on the MF signal in the form of the inner and outer walls of the pipeline is also compared, and the conclusion that the RFEC has the same sensitivity to the detection of the inner and outer wall defects of the pipeline is confirmed. The RFEC detection system is built, and through the comparative experiment of defect detection of different types of receiving coils, it is concluded that the small receiving coils with the coil center axis parallel to the pipe axis and placed close to the inner wall of the pipe are the best form of receiving coils for MF signals. According to the most representative three types of defects on the pipe wall, it is found that the circumferential extension defects are the easiest to be detected, and the axial extension defects are the most difficult to be detected. The relationship between the defect depth and the voltage amplitude and phase of the detection signal is analyzed. It is found that the defect depth has an approximate exponential relationship with the amplitude of the detection signal and an approximate proportional relationship with the signal phase.

Compared with other methods, this method has higher reliability and validity in pipeline detection, and has the same sensitivity in detecting defects on the inner and outer walls of pipelines. At the same time, there is still a lot of work to be done in the future: (1) Conventional eddy current can also be applied to tube wall defect detection. This paper only studied the relationship between the signal in the remote field and the defect, but it remains to be studied whether the signal in the near field similar to conventional eddy current can also be helpful to defect detection. (2) During the experimental operation, it was found that when the running speed of the probe in the tube was different, the defect signals obtained were different, which could be studied and analyzed later. (3) In the experimental operation, it was also found that when the probe moves in different directions, namely, the excitation coil is first close to the pipe wall defect and the receiving coil is first close to the pipe wall defect, the defect signals obtained were also different. How to identify defects more effectively is worthy for further study.

## Acknowledgments

This work was support by the National Natural Science Foundation of China (Grant: 21204139), the open Fund of Key Laboratory of Oil &Gas Equipment, Ministry of Education (Southwest Petroleum University) (Grant: OGE 201701-03), the State Key Laboratory of Oil and Gas

Reservoir Geology and Exploitation (Southwest Petroleum University) (Grant: PLN201829).

## References

[1] G. M. Javier, G. G. Jaime, and V. S. Ernesto, Sensors **3**, 11 (2011).
[2] K. Noriyasu, U. Souichi, N. Satoshi, O. Makoto, and J. Noboru, ICONE-18, Nucl. Eng. Des, Xian (2010) pp. 4643-4648.
[3] B. Yang, J. Xu, H. Wu, and Y. He, Ndt and E International **10**, 90 (2017).
[4] J. W. Park, J. H. Park, S. J. Song, M. B. Kishore, S. G. Kwon, and H. J. Kim, J. Magn. **4**, 22 (2017).
[5] K. J. Kim, J. Park, and J. Y. Park, J. Magn. **1**, 23 (2018).
[6] J. Liu, H. Zheng, Y. Kuang, X. Xu, and Y. Liu, Mechanika **4**, 24 (2018).
[7] B. Yang, H. Zhang, C. Zhang, and Z. Zhang, Nondestruct. Test Eva. **4**, 28 (2013).
[8] X. Xu, M. Liu, Z. Zhang, and Y. Jia, Sensors **12**, 14 (2014).
[9] L. Pacheco, Javier, and M. M. Pilar, Sensors **2**, 15 (2015).
[10] R. Grimberg, L. Udpa, A. Savin, R. Steigmann, P. vizureanu, A. Bruma, and S. Udpa, Research in Nondestructive Evaluation **4**, 19 (2008).
[11] B. F. Yang and X. C. Li, Nondestruct. Test Eva. **1**, 25 (2010).
[12] D.Vasic, V. Bilas, and D. Ambrus, IEEE Trans Instrum. **2**, 53 (2004).
[13] S. M. Haugland, IEEE T Magn. **4**, 32 (1996).
[14] P. Chen and P. Huang, PIERS, Electromagnet Acad, St Petersburg (2017) pp 1898-1905.
[15] W. Lord, Y. S. Sun, S. S. Udpa, and S. Nath, IEEE T Magn. **2**, 24 (1988).
[16] K. H. Min, Y. H. Ryong, and P. G. Soo, IEEE T Magn. **11**, 54 (2018).
[17] D. Vasic, V. Bilas, and D. Ambrus, IMTC 2003, CO, USA (2003) pp 20-22.
[18] J. Wang, N. Yusa, H. P, T. Takagi, and H. Hashizume, Mater. Trans. **1**, 54 (2013).
[19] D. L. Atherton, IEEE T Magn. **6**, 31(1995).
[20] D. Kim, L. Udpa, and S. Udpa, Mater. Lett. **3**, 58 (2004).
[21] Y. J. Kim and S. S. Lee, Ndt. and E International **1**, 49 (2012).
[22] H. T. Wang, Q. F. Luo, X. Wang, G. Y. Tian, L. D. Xing, P. Wang, and Y. Li, Int. J. Appl. Electrom. **3**, 33 (2010).
[23] Y. L. Diraison, P. Y. Joubert, and D. Placko, Ndt and E International **2**, 42 (2009).